NIST Author Manuscript

NIST Author Manuscript

NIST Author Manuscript

Author Manuscript

Accepted for publication in a peer-reviewed journal

NIST National Institute of Standards and Technology • U.S. Department of Commerce

Published in final edited form as:

J Chem Eng Data. 2018 ; 63: . doi:10.1021/acs.jced.8b00132.

Measurement and Correlation of the Thermal Conductivity of 1,1,1,2,2,4,5,5,5-Nonafluoro-4-(trifluoromethyl)-3-pentanone[†,§]

Richard A. Perkins[*],

Thermophysical Properties of Fluids Group, National Institute of Standards and Technology, 325 Broadway, Boulder, Colorado, 80305-3337, United States

Marcia L. Huber, and

Thermophysical Properties of Fluids Group, National Institute of Standards and Technology, 325 Broadway, Boulder, Colorado, 80305-3337, United States

Marc J. Assael

Laboratory of Thermophysical Properties and Environmental Processes, Chemical Engineering Department, Aristotle University, Thessaloniki 54636, Greece

Abstract

New experimental data for the thermal conductivity of 1,1,1,2,2,4,5,5,5-nonafluoro-4-(trifluoromethyl)-3-pentanone (Novec 649) are reported for vapor, liquid and supercritical states. These new experimental data were obtained with transient hot-wire apparatus over the temperature range from 183 K to 501 K and at pressures from 0.02 MPa to 69 MPa. These data were used to develop a wide-range correlation for the thermal conductivity of the vapor, liquid and supercritical fluid. The experimental data reported here have an uncertainty of 1 % for the liquid and supercritical regions (densities > 600 kg m^{-3}), 1.5 % for vapor and supercritical regions (pressures ≥1 MPa and densities < 200 kg m^{-3}), 3 % for supercritical states (200 kg m^{-3} ≤densities ≤600 kg m^{-3}), and 3 % for vapor and supercritical states (pressures < 1 MPa). The thermal-conductivity correlation developed in this work is estimated to have an expanded relative uncertainty, at a 95 % confidence level, ranging from approximately 1 % to 4 % that depends upon the temperature and pressure, with larger uncertainties in the critical region.

Graphical Abstract

[†]Contribution of the National Institute of Standards and Technology, not subject to United States copyright.

[§]Commercial equipment, instruments, or materials are identified only to adequately specify certain procedures. Such identification does not imply recommendation or endorsement by the National Institute of Standards and Technology, nor does it imply that the identified products are necessarily the best available for the purpose.

[*]**Corresponding Author:** richard.perkins@nist.gov. Tel.: +1-303-497-5499. Fax: +1-303-497-6682.

Supporting Information

Tabulated experimental values (69 pages) are reported in the supporting information and are available athttp://pubs.acs.org.

The authors declare no competing financial interest.

NIST Author Manuscript

NIST Author Manuscript

NIST Author Manuscript

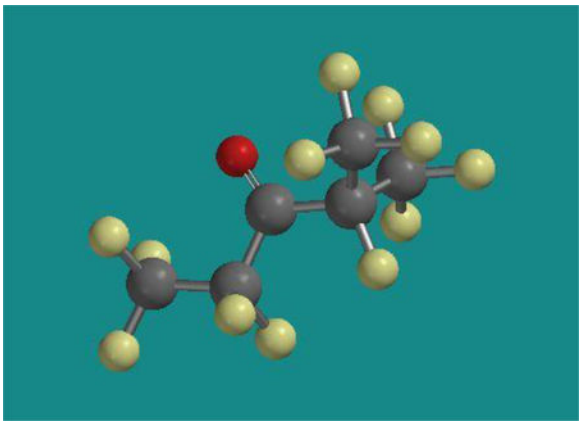

1. INTRODUCTION

The chemical 1,1,1,2,2,4,5,5,5-nonafluoro-4-(trifluoromethyl)-3-pentanone, also known as Novec 649, Novec 1230, and FK-5-1-12, is a fully fluorinated ketone that is under development for applications as a working fluid in Organic Rankine Cycles,[1] as a working fluid in electronics cooling applications,[2, 3] and as a replacement agent in fire suppression systems.[4–6] In the heat transfer community, it is typically known as Novec 649, while in the fire suppression community it is usually called Novec 1230 or FK-5-1-12. In this manuscript, for convenience, we will refer to this fluid as Novec 649. It has a CAS number of 756-13-8 and chemical formula $C_6F_{12}O$ with molar mass 316.0444 g mol^{-1}. Much of the interest in Novec 649 arises from the fact that it has zero ozone depletion potential (ODP) and an atmospheric lifetime of 1–2 weeks, resulting in a global warming potential (GWP) that is negligible.[7]

McLinden et al.[8] reported comprehensive thermodynamic property measurements (density, sound speed, and vapor pressure) and developed an equation of state (EOS) explicit in Helmholtz energy for Novec 649 that we use in this work for thermodynamic properties. The EOS is valid from the triple point to 500 K at pressures up to 50 MPa and has uncertainties in liquid density of 0.05 % from 220 K to 440 K at pressures to 40 MPa. In addition, we adopt the critical temperature, pressure, and density consistent with this EOS, namely 441.81 K, 1.869 MPa, 606.81 kg m^{-3}. Tanaka[9] reported additional pressure-density-temperature measurements with an emphasis on the near-critical and supercritical region. More recently, Wen et al.[10] measured the viscosity and presented a correlation for viscosity based on their measurements. We are unaware of any published data on the thermal conductivity of Novec 649.

In this manuscript, wide-ranging measurements for the thermal conductivity of Novec 649 are reported for liquid, vapor, and supercritical states with temperatures ranging from 183 K to 501 K and with pressures up to 69 MPa. Based on these thermal conductivity data, we developed a correlation for Novec 649 that is valid over the vapor, liquid, and supercritical regions.

NIST Author Manuscript NIST Author Manuscript NIST Author Manuscript

2. EXPERIMENTAL SECTION

2.1. Sample Material.

The Novec 649 sample was supplied by 3M. This same sample was also used for determination of density, speed of sound, and vapor pressure in a separate study.[8] It was reported by the supplier to have a purity of 0.9998 mole fraction on an organic basis with a nonvolatile residue of 1×10^{-6} mole fraction. Our own analysis by GC-mass spectrometry and infrared spectrometry, following the protocols of Bruno and Svoronos,[11, 12] indicated a purity of 0.9995 mole fraction with 0.0005 mole fraction of 1,1,1,2,3,3,3-heptafluoropropane, and a water content that was determined by Karl Fischer titration to be less than 25×10^{-6} mole fraction. The sample was degassed by multiple freeze-thaw cycles in liquid nitrogen with evacuation of the vapor space until the final pressure over the frozen sample was 5×10^{-3} Pa. The sample characterization is summarized in Table 1.

2.2. Hot-Wire Systems.

The thermal conductivity was measured with two different hot-wire systems that cover the entire temperature range. The low-temperature system measures thermal conductivity at temperatures from 60 K to 345 K. The low-temperature cell is copper with a sample volume of 25 ml and has two hot wires that eliminate axial conduction effects. The high-temperature system measures thermal conductivity at temperatures from 300 K to 750 K and can be used with both single-wire and double-wire cells. The high-temperature single-wire cell that was used for the Novec 649 measurements reported here had a small-volume of 5 ml and was made from 316 stainless steel.. In both hot-wire cells, small platinum hot wires of 12.7 μm diameter serve to approximate line-source electrical heaters, while functioning as resistance thermometers to measure the temperature rise during each experiment. The resistance of each of the hot wires is calibrated in-situ as a function of the measured temperature and pressure so measurement of resistance increase allows the temperature increase to be determined. Both hot-wire systems were operated in transient or steady-state modes depending upon the fluid state. Both hot-wire apparatus were used for experimental determination of the thermal conductivity of the liquid, vapor, or supercritical fluid states of Novec 649. Steady-state measurements have lower uncertainty for dilute-gas measurements due to increasingly more significant corrections to transient measurements for finite wire diameter and penetration to the outer boundary, which depend upon the increasing thermal diffusivity of the gas with decreasing pressure at low pressures.

At temperatures below 345 K, the thermal conductivity was measured with the low-temperature cryostat system.[13] The temperature of this hot-wire cell controlled with a multilayer copper cryostat that is cooled by immersion in liquid nitrogen. The two hot-wires are supported at the top of their respective cylindrical cavities of 9 mm diameter and tensioned with small weights at the bottom end. The difference between the response of the long and short hot wires is recorded from the response of a Wheatstone bridge. The recorded bridge signal is effectively from the central portion of the long wire with the two half-lengths of the short wire response removed. It is this region, near the wire end supports, where axial temperature gradients exist during an experiment. The initial cell temperatures, T_i, is measured with an expanded uncertainty of $U(T_i)$=0.005 K with a platinum resistance

NIST Author Manuscript

NIST Author Manuscript

NIST Author Manuscript

thermometer. The fluid pressure, P_e, is determined with a quartz pressure transducer with an expanded uncertainty of $U(P_e)$=7 kPa over the pressure range from (0 to 70) MPa.

At temperatures above 345 K, the thermal conductivity was measured with a high-temperature thermostat system. The thermostat consists of a DC powered furnace with an isothermal shield that encloses the hot-wire cell. The single platinum hot wire is supported at the top and tensioned with a spring arrangement at the bottom in a commercial microreactor with an 8 mm diameter bore. A Wheatstone bridge circuit is used to measure the resistance increase and temperature rise of the wire as in the low-temperature cryostat system. The correction for axial conduction during data analysis for the single-wire cell is based on the model of Woodfield et al.[14] The initial cell temperature, T_i, is measured with an expanded uncertainty of $U(T_i)$=0.005 K with a platinum resistance thermometer. The fluid pressure, P_e, is determined with a quartz pressure transducer with an expanded uncertainty of $U(P_e)$=7 kPa over the pressure range from (0 to 70) MPa. All reported expanded uncertainties are for a coverage factor of k=2, approximately a 95 % confidence interval.

2.3. Transient Measurements.

Both hot-wire systems used in the present measurements were designed based upon the early work of Healy *et al.*[15] In this approach, the ideal temperature rise, ΔT_{id}, is given by

$$\Delta T_{id} = \frac{q}{4\pi\lambda}\left[\ln(t) + \ln\left(\frac{4a}{r_0^2 C}\right)\right] = \Delta T_W + \sum_{i=1}^{10} \delta T_i, \quad (1)$$

where q is the applied power per unit length, λ is the fluid thermal conductivity, t is the time elapsed after application of power, $a = \lambda/(\rho C_p)$ is the fluid thermal diffusivity, ρ is the fluid density, C_p is the fluid isobaric specific heat capacity, r_0 is the hot-wire radius, and C is the exponential of Euler's constant. The ideal temperature rise is related to the measured temperature rise of the wire, ΔT_w, and the summation of the temperature rise corrections, δT_i.[15] The thermal conductivity can be found from the slope a plot of ΔT_{id} as a function of $\ln(t)$ and the thermal diffusivity can be found from the intercept. During data analysis, a line is fit to Eq. 1 over an optimum time interval, typically from 0.1 s to 1.0 s where the magnitude of the corrections remain small. In the present work we only consider the thermal conductivity from the slope of the fit line. The experimental temperature, T_e, associated with the thermal conductivity is the average wire temperature over the time interval that was fit for each experiment.

Four corrections were found to be significant during the present measurements on Novec 649. The correction accounting for the finite diameter and heat capacity of the hot wire was generally the largest for both gas and liquid measurements at short experiment times of less than 0.1 s. As discussed above, the correction for finite wire length is not required for the low-temperature double-wire cell but is required for the high-temperature single-wire cell. The correction for finite wire length remains small relative to the finite wire diameter and outer boundary corrections for wires with a large length to diameter ratio like those used in

NIST Author Manuscript

NIST Author Manuscript

NIST Author Manuscript

the present work. The full heat correction for finite wire diameter[15] was applied to the present measurements.

Depending upon the thermal diffusivity of the gas and experiment elapsed time, it is possible for the transient temperature gradient to penetrate to the cavity wall during measurements on dilute-gas samples.[14–19] Thus, the outer boundary correction also becomes very significant for such dilute-gas samples. The end time for the fit interval was determined such that fluid convection was not significant, especially significant for measurements in the critical region, and the outer boundary correction remained small during dilute-gas measurements. An experiment duration of 1 s was considered optimal for most transient experiments in the vapor, liquid and supercritical states. A few dilute-gas experiments required reduction of the upper fit limit to times less than 1 s due to the large fluid thermal diffusivity, as did a few experiments near the gas-liquid critical point due to increasing fluid convection.

For small temperature rises, the thermal radiation correction is approximately proportional to T^3 (T_1-T_2), so in the present hot-wire experiments the thermal radiation correction and remains relatively small at temperatures up to 500 K. The transparent fluid correction[15] was applied for the present measurements in both the gas and liquid phases.

2.4. Steady-State Measurements.

Earlier work has demonstrated that steady-state hot-wire measurements are reliable and require smaller corrections than transient hot-wire measurements for dilute-gas samples.[14, 20] The steady-state solution of Fourier's law for concentric cylinders gives the fluid thermal conductivity, λ,

$$\lambda = \frac{q \ln\left(\frac{r_2}{r_1}\right)}{2\pi(T_1 - T_2)}, \quad (2)$$

in terms of the cell geometry and temperature rise for a given applied power per unit length, q. In Eq. 2, r_1 and T_1 are the radius and temperature of the hot wire, while r_2 and T_2 are the radius and temperature of the concentric cylindrical cavity containing the fluid. The temperature T_2 is assumed to be constant at the initial cell temperature measured with the platinum resistance thermometer due to the large mass and heat capacity of the cell.

Detailed discussion of steady-state measurements of dilute gases with transient hot-wire systems is given by Roder et al.[20] Fluid convection corrections increase with increasing pressure and density in the dilute gas but remain small at pressures below 0.7 MPa. The transparent fluid correction for thermal radiation is applied in the present work. The correction for eccentricity between the hot wire and the outer boundary remains small due to the small wire diameter.

NIST Author Manuscript NIST Author Manuscript NIST Author Manuscript

3. EXPERIMENTAL RESULTS

The thermal conductivity data for Novec 649 are available in the Supporting Information. At each initial state point, there are generally five transient or steady-state experimental results at different applied powers. The Helmholtz equation of state of McLinden et al.[8] was used to calculate the densities reported in the Supporting Information and for the corrections required during analysis of the hot-wire temperature rise data at each measured temperature and pressure. The temperature and pressure range covered by the present measurements is shown in Figure 1 along with the saturation boundary for Novec 649.[8] There were 99 transient vapor and 735 transient liquid measurements at temperatures from 183 K to 334 K, with pressures up to 69.2 MPa, reported from the low-temperature double-wire instrument. There were 412 steady-state vapor, 264 transient vapor, 633 transient liquid measurements at temperatures from 301 K to 501 K reported from the high-temperature single-wire instrument. There were 623 transient supercritical measurements at temperatures from 434 K to 500 K reported from the high-temperature single-wire instrument. The average temperatures of the 7 transient vapor isotherms were (345, 360, 375, 389, 403, 417, and 433) K. The average temperatures of the 10 steady-state vapor isotherms were (301, 315, 330, 344, 359, 374, 388, 403, 417, and 433) K. Three supercritical isotherms at (454, 473, and 500) K were measured in both transient and steady-state modes. The average temperatures of the 12 liquid isotherms were (184, 192, 213, 243, 273, 302, 330, 332, 359, 390, 417, and 433) K. Figure 2 shows the measured thermal conductivity data as a function of the calculated density. The critical enhancement is significant near the critical density for the subcritical and supercritical isotherms near the critical point. Figure 2 shows the strong dependence of the thermal conductivity on density that will be the basis of the correlation described below.

For the low-temperature double-wire cell, the expanded uncertainty of the reported thermal conductivity is 3 % for the gas phase at pressures below 1 MPa and 1 % for the liquid-phase measurements. For the high-temperature single-wire cell, the expanded uncertainty of the reported thermal conductivity is 1.5 % for the vapor and supercritical measurements at pressures above 1 MPa and densities below 200 kg m^{-3}, 3 % for gas measurements at pressures less than 1 MPa and for the supercritical isotherms over the density range 200 kg m^{-3} $\leq \rho_e \leq$ 600 kg m^{-3}. The expanded uncertainty is 1 % for the liquid phase and supercritical measurements from the high-temperature single-wire cell at densities above 600 kg m^{-3}.

The steady-state thermal conductivity data have an expanded uncertainty of 3 %. All steady-state measurements are gas at low pressures (less than 0.7 MPa). In the Supporting Information, the tables of steady-state data provide the calculated Rayleigh number that characterizes the level of convection during each experiment.

4. THERMAL CONDUCTIVITY CORRELATION

The thermal conductivity λ is represented as a sum of three contributions,

NIST Author Manuscript

NIST Author Manuscript

NIST Author Manuscript

$$\lambda(\rho, T) = \lambda_0(T) + \Delta\lambda_r(\rho, T) + \Delta\lambda_c(\rho, T), \quad (3)$$

where λ_0 is the thermal conductivity of the dilute-gas that depends only on temperature, $\Delta\lambda_r$ is the residual thermal conductivity that depends strongly on density and more weakly on temperature, and $\Delta\lambda_c$ is the thermal conductivity critical enhancement that increases dramatically in the critical region. Both $\Delta\lambda_r$ and $\Delta\lambda_c$ are functions of temperature, T, and molar density, ρ, with ρ calculated with an equation of state for each experimental T and P. In this work, we use the Helmholtz equation of state of McLinden et al.[8] that is valid at temperatures from 165 K to 500 K with pressures up to 50 MPa. Some experimental conditions in this work exceed 50 MPa and we use extrapolated results from the EOS to provide densities at pressures between 50 and 69 MPa.

4.1. Dilute-gas thermal conductivity.

The dilute-gas thermal conductivity of Novec 649 is represented as a rational polynomial in reduced temperature,

$$\lambda_0(T_r)/(\mathrm{W \cdot m^{-1} \cdot K^{-1}}) = \frac{\sum_{k=0}^{5} A_k (T_r)^k}{\sum_{j=0}^{3} a_j (T_r)^j}, \quad (4)$$

with coefficients A_k and a_j, where T_r is the reduced temperature T/T_c where T is the temperature and T_c is the critical temperature. Eq. 4 has been shown to extrapolate well to high temperatures, as needed for Novec 649, which may have applications in fire suppression studies that extend to high temperatures.

4.2. Residual thermal conductivity.

A polynomial in temperature and density is used to represent the residual, contribution to the thermal conductivity of Novec 649,

$$\Delta\lambda_r(\rho, T) \,/\, (\mathrm{W \cdot m^{-1} \cdot K^{-1}}) = \sum_{i=1}^{5} \left(B_{i,1} + B_{i,2}\left(\frac{T}{T_c}\right) \right) \left(\frac{\rho}{\rho_c}\right)^i, \quad (5)$$

with coefficients $B_{i,j}$, where ρ is the molar density and ρ_c is the critical density. This functional form has been used successfully to represent the thermal conductivity of several alternative refrigerants such as the hydrofluoroolefins R1234yf,[21] R1234ze(E),[21] and R1233zd(E).[22]

4.3. Critical Enhancement.

The theoretically based mode-coupling theory of Olchowy and Sengers[23] accurately describes the thermal conductivity enhancement in the critical region. A simplified version of their crossover model[24] is used for the thermal conductivity of Novec 649,

NIST Author Manuscript NIST Author Manuscript NIST Author Manuscript

$$\Delta\lambda_c(T,\rho) / (\mathrm{W}\cdot\mathrm{m}^{-1}\cdot\mathrm{K}^{-1}) = \frac{\rho C_p R_0 k_B T}{6\pi\eta\xi}\left(\Omega - \Omega_0\right), \quad (6)$$

where the isobaric heat capacity, $C_p(T,\rho)$, is obtained from the equation of state,[8] k_B is Boltzmann's constant, $R_0 = 1.02$ is a universal constant,[25] and the viscosity, $\eta(T,\rho)$, is obtained from the recent correlation of Wen et al.[10] In Eq. (6), ρ is in mol· m^{-3}, C_p is in J mol^{-1}, k_B is in J K^{-1}, T in K, η is in Pa s, and the correlation length ξ defined below is in m.

The crossover functions Ω and Ω_0 in Eq. 6 also depend upon the correlation length and are given by

$$\Omega = \frac{2}{\pi}\left[\left(\frac{C_p - C_V}{C_p}\right)\arctan(q_d\xi) + \frac{C_V}{C_p}(q_d\xi)\right], \quad (7)$$

$$\Omega_0 = \frac{2}{\pi}\left[1 - \exp\left(\frac{-1}{(q_d\xi)^{-1} + \frac{1}{3}\left(\frac{(q_d\xi)\rho_c}{\rho}\right)^2}\right)\right]. \quad (8)$$

The isochoric heat capacity, $C_V(T,\rho)$, is obtained from the equation of state (EOS), and the correlation length ξ is given by

$$\xi = \xi_0\left[\frac{P_c\rho}{\Gamma\rho_c^2}\right]^{\nu/\gamma}\left[\left.\frac{\partial\rho(T,\rho)}{\partial P}\right|_T - \frac{T_R}{T}\left.\frac{\partial\rho(T_R,\rho)}{\partial P}\right|_T\right]^{\nu/\gamma}, \quad (9)$$

where the critical amplitudes Γ and ξ_0 are system-dependent and are determined by the asymptotic behavior of the equation of state in the critical region. The partial derivative $\partial\rho/\partial P|_T$ is evaluated with the equation of state at the system temperature T and at a reference temperature, T_R. For the reference temperature, we select a value where the critical enhancement is found to be negligible: $T_R = 1.5\,T_c$. The exponents $\gamma = 1.239$ and $\nu = 0.63$ are universal constants.[24] We have used fluid specific values of the critical amplitudes calculated from the generalized method of Perkins et al.,[26] $\Gamma = 0.061$ and $\xi_0 = 2.51\times10^{-10}$ m. The cutoff wave number q_d (or, alternatively, its inverse, q_d^{-1}) is sensitive to thermal conductivity data in the critical region and is fit to the present Novec 649 thermal conductivity data.

4.4. Data Fitting.

We first fit the dilute-gas measurements to obtain the coefficients of the dilute gas in the limit of zero density, Eq. 4. The data for gas-phase isotherms were extrapolated to zero

NIST Author Manuscript NIST Author Manuscript NIST Author Manuscript

density, and these points, along with some estimated points at high temperatures (up to 1000 K) obtained from the procedure described in our previous work,[27] were fit to obtain the values in Table 2. The complete experimental data set, with the dilute-gas coefficients fixed, was then fit with the fitting program ODRPACK[28] to obtain the coefficients B_{ij} in Eq. 5, given in Table 1, and the value of q_d^{-1} for the critical enhancement in Eqs. (6–9). We found q_d^{-1} = 0.334 nm. The value obtained from the predictive scheme of Perkins et al.[26] is 0.798 nm. This is a larger discrepancy than we typically see, and we think that it is possible that the critical point used in the equation of state of McLinden et al.[8] may be inaccurate. Tanaka[9] observed large deviations of his data from the EOS of McLinden et al.[8] when very close to the critical point, and this may also be due to inaccuracies in the reported location of the critical point. Additional experimental verification of the critical point would be valuable.

The validity of the fitted coefficients in Table 2 was checked by comparisons of the standard deviation of each coefficient relative to the coefficient itself. In all cases, the standard deviation was 5 to 10 times smaller than the coefficient. The behavior of the correlation was examined and found to be smooth with reasonable extrapolation behavior beyond the temperature and density range of available data. Table 3 provides calculated values of the thermal conductivity at several temperatures and pressures that allow readers to verify computer coding of the correlation reported here. Values of pressure shown in Table 3 are computed from the equation of state of McLinden et al.[8] at the specified temperatures and densities in Table 3.

4.5. Data Deviations.

The present work reports 2766 measurements of thermal conductivity of Novec 649 in the liquid, gas, and supercritical regions from T=183 K to 501 K at pressures to 69 MPa. Figure 3 shows deviations between the present measurements and the correlation reported above as a function of density for the gas phase over the temperature range from 300 K to 500 K with pressures less than 1 MPa. Figure 4 shows the deviations between the present measurements and the correlation over the entire density range of the measurements at temperatures from 183 K to 501 K with pressures up to 69 MPa. Figures 5 and 6 show deviations between all the thermal conductivity data and the correlation as a function of measured temperature and pressure, respectively. The gas-phase data at pressures up to 1 MPa have an average absolute deviation (AAD) of 1.8 % for both the transient and steady-state measurements. We estimate the expanded uncertainty of the correlation in this region to be 4 % at a 95 % confidence level. The average absolute deviation between the measurements and the correlation is 0.5 % and the expanded uncertainty is estimated to be 1 % for the liquid phase at pressures up to 69 MPa over the temperature range 183 K to 434 K. For the supercritical region, we estimate the uncertainty to be 4 % for densities below 200 kg m^{-3}, 3 % for intermediate densities between 200 and 800 kg m^{-3}, and 1 % for densities above 800 kg m^{-3}. The correlation represents the data at pressures to 70 MPa in a physically reasonable way even at pressures that exceed the recommended upper pressure limit (50 MPa) of the equation of state of McLinden et al.[8]

NIST Author Manuscript

NIST Author Manuscript

NIST Author Manuscript

5. CONCLUSIONS

A total of 2766 points are reported for the thermal conductivity of Novec 649 in the liquid, gas, and supercritical regions at pressures to 69 MPa. The experimental data reported here have an expanded uncertainty at a 95 % confidence level of 1 % for liquid measurements increasing to 3 % for gas at low pressures (less than 1 MPa) and in the critical region. Based on these measurements, a correlation is developed for the thermal conductivity surface of Novec 649 covering the liquid, gas, and supercritical regions that may be used from the triple point to 500 K and pressures up to 70 MPa.

Supplementary Material

Refer to Web version on PubMed Central for supplementary material.

ACKNOWLEDGEMENTS

We thank Paul Stempko and Dele Fayemi of 3M for the sample of Novec 649 studied in the present work. We thank Mark McLinden of NIST for sample preparation that included the freeze-thaw degassing of the sample. We thank Tom Bruno and Tara Lovestead of NIST for characterization of the sample purity.

REFERENCES

1. Ghim G; Lee J Condensation heat transfer of low GWP ORC working fluids in a horizontal smooth tube. Int. J. Heat Mass Trans 2017, 104, 718–728.
2. Gess JL; Bhavnani SH; Johnson W Experimental Investigation of a Direct Liquid Immersion Cooled Prototype for High Performance Electronic Systems. IEEE Trans. Comp. Pack. Mfg. Technol 2015, 5, 1451–1464.
3. Kearney DJ; Suleman O; Griffin J; Mavrakis G Thermal performance of a PCB embedded pulsating heat pipe for power electronics applications. Appl. Thermal Eng 2016, 98, 798–809.
4. Hulse RJ; Basu RS; Singh RR; Thomas RHP Physical Properties of HCFO-1233zd(E). J. Chem. Eng. Data 2012, 57, 3581–3586.
5. Gatsonides JG; Andrews GE; Phylaktou HN; Chattaway A Fluorinated halon replacement agents in explosion inerting. J. Loss Prev. Proc. Ind 2015, 36, 546–554.
6. Pagliaro JL; Linteris GT; Sunderland PB; Baker PT Combustion inhibition and enhancement of premixed methane-air flames by halon replacements. Combust. and Flame 2015, 162, 41–49.
7. Taniguchi N; Wallington TJ; Hurley MD; Guschin AG; Molina LT; Molina MJ Atmospheric chemistry of C2F5C(O)CF(CF3)(2): Photolysis and reaction with Cl atoms, OH radicals, and ozone. J. Phys. Chem. A 2003, 107, 2674–2679.
8. McLinden MO; Perkins RA; Lemmon EW; Fortin TJ Thermodynamic Properties of 1,1,1,2,2,4,5,5,5-Nonafluoro-4-(trifluoromethyl)-3-pentanone: Vapor Pressure, (p, ρ, T) Behavior, and Speed of Sound Measurements, and an Equation of State. J. Chem. Eng. Data 2015, 60, 3646–3659.
9. Tanaka K Measurement of p ρ T Properties of 1,1,1,2,2,4,5,5,5-Nonafluoro-4-(trifluoromethyl)-3-pentanone in the Near-Critical and Supercritical Regions. J. Chem. Eng. Data 2016, 61, 3958–3961.
10. Wen C; Meng X; Huber ML; Wu J Measurement and Correlation of the Viscosity of 1,1,1,2,2,4,5,5,5-Nonafluoro-4-(trifluoromethyl)-3-pentanone. J. Chem. Eng. Data 2017, 62, 3603–3609. [PubMed: 29311751]
11. Bruno TJ; Svoronos PDN CRC Handbook of Basic Tables for Chemical Analysis; Taylor and Francis CRC Press: Boca Raton, FL, 2011.
12. Bruno TJ; Svoronos PDN, CRC Handbook of Fundamental Spectroscopic Correlation Charts; Taylor and Francis CRC Press: Boca Raton, FL, 2005.

NIST Author Manuscript NIST Author Manuscript NIST Author Manuscript

13. Roder HM A Transient Hot Wire Thermal Conductivity Apparatus for Fluids. J. Res. Natl. Bur. Stand. 1981, 86, 457–493.
14. Woodfield PL; Fukai J; Fujii M; Takata Y; Shinzato K A Two-Dimensional Analytical Solution for the Transient Short-Hot-Wire Method. Int. J. Thermophys 2008, 29, 1278–1298.
15. Healy JJ; DeGroot JJ; Kestin J The Theory of the Transient Hot-Wire Method for Measuring the Thermal Conductivity. Physica 1976, 82C, 392–408.
16. Assael MJ; Karagiannidis L; Richardson SM; Wakeham WA Compression Work using the Transient Hot-Wire Method. Int. J. Thermophys 1992, 13, 223–235.
17. Taxis B; Stephan K Application of the transient hot-wire method to gases at low pressures. Int. J. Thermophys 1994, 15, 141–153.
18. Li SFY; Papadaki M; Wakeham WA The measurement of the Thermal Conductivity of Gases at Low Density by the Transient Hot-Wire Technique. High Temp. High Press 1993, 25, 451–458.
19. Li SFY; Papadaki M; Wakeham WA Thermal Conductivity of Low-Density Polyatomic Gases In Thermal Conductivity 22, Tong TW, Ed.; Technomic Publishing: Lancaster, PA, 1994; pp 531–542.
20. Roder HM; Perkins RA; Laesecke A; Nieto de Castro CA Absolute steady-state thermal conductivity measurements by use of a transient hot-wire system. J. Res. .Natl. Inst. Stand. Tech 2000, 105, 221–253.
21. Perkins RA; Huber ML Measurement and correlation of the thermal conductivity of 2,3,3,3-tetrafluoroprop-1-ene (R1234yf) and trans-1,3,3,3-tetrafluoropropene (R1234zd(E). J. Chem. Eng. Data 2011, 56, 4868–4874.
22. Perkins RA; Huber ML; Assael MJ Measurement and Correlation of the Thermal Conductivity of trans-1-Chloro-3,3,3-trifluoropropene (R1233zd(E)). J. Chem. Eng. Data 2017, 62, 2659–2665. [PubMed: 29230068]
23. Olchowy GA; Sengers JV Crossover from Regular to Singular Behavior of the Transport Properties of Fluids in the Critical Region. Phys. Rev. Lett 1988, 61, 15–18. [PubMed: 10038682]
24. Olchowy GA; Sengers JV A Simplified Representation for the Thermal Conductivity of Fluids in the Critical Region. Int. J. Thermophys 1989, 10, 417–426.
25. Krauss R; Weiss VC; Edison TA; Sengers JV; Stephan K Transport Properties of 1,1-Difluoroethane (R152a). Int. J. Thermophys 1996, 17, 731–757.
26. Perkins RA; Sengers JV; Abdulagatov IM; Huber ML Simplified model for the critical thermal-conductivity enhancement in molecular fluids. Int. J. Thermophys 2013, 34, 191–212.
27. Tsolakidou CM; Assael MJ; Huber ML; Perkins RA Correlations for the Viscosity and Thermal Conductivity of Ethyl Fluoride (R161). J. Phys. Chem. Ref. Data 2017, 46, 023103. [PubMed: 28785120]
28. Boggs PT, Byrd RH, Rogers JE, Schnabel RB ODRPACK, Software for Orthogonal Distance Regression; NISTIR 4834; National Institute of Standards and Technology: Gaithersburg, MD USA, 1992.

NIST Author Manuscript

NIST Author Manuscript

NIST Author Manuscript

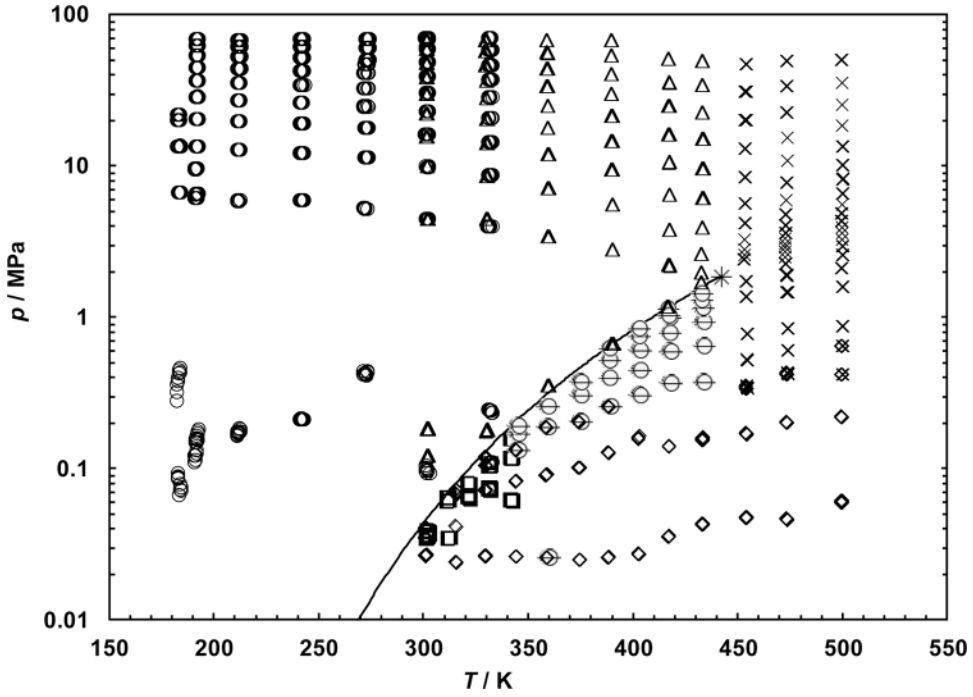

Figure 1.

Distribution of the data for the thermal conductivity of Novec 649:, double-wire transient vapor; ◇, double-wire steady-state vapor; O, double-wire transient liquid;×, single-wire supercritical; ⊖, single-wire transient vapor; Δ, single-wire transient liquid. The solid line shows the vapor-liquid saturation boundary, terminating at the critical point,✳

NIST Author Manuscript

NIST Author Manuscript

NIST Author Manuscript

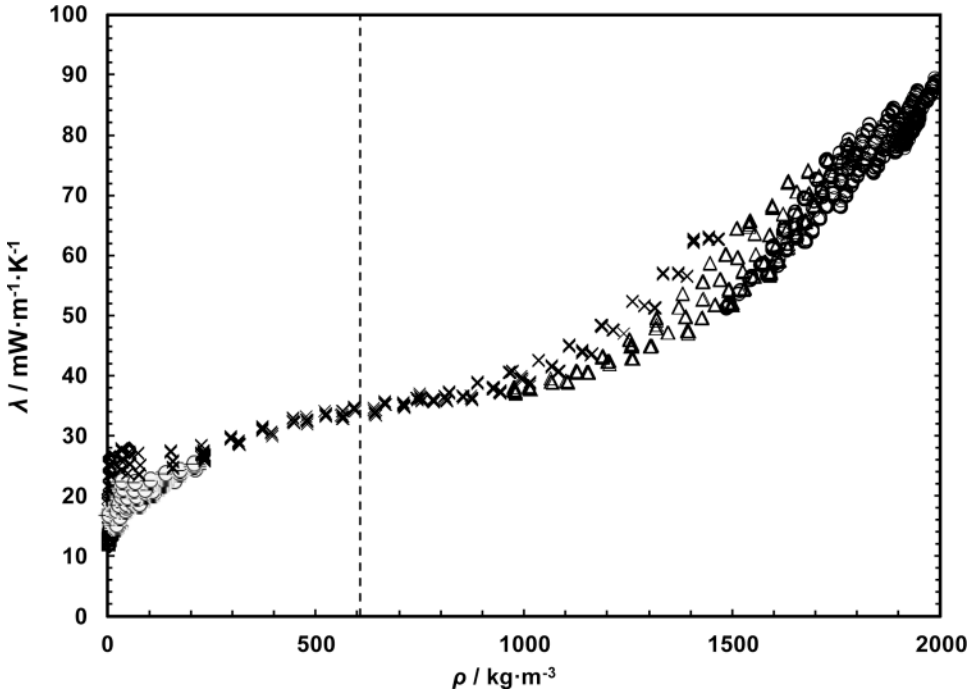

Figure 2.

Thermal conductivity of Novec 649 as a function of the density calculated at the measured temperature and pressure:, double-wire transient vapor; ◇, double-wire steady-state vapor; O, double-wire transient liquid;×, single-wire supercritical; ⊖, single-wire transient vapor; Δ, single-wire transient liquid. The critical density is indicated by the dashed line.

NIST Author Manuscript

NIST Author Manuscript

NIST Author Manuscript

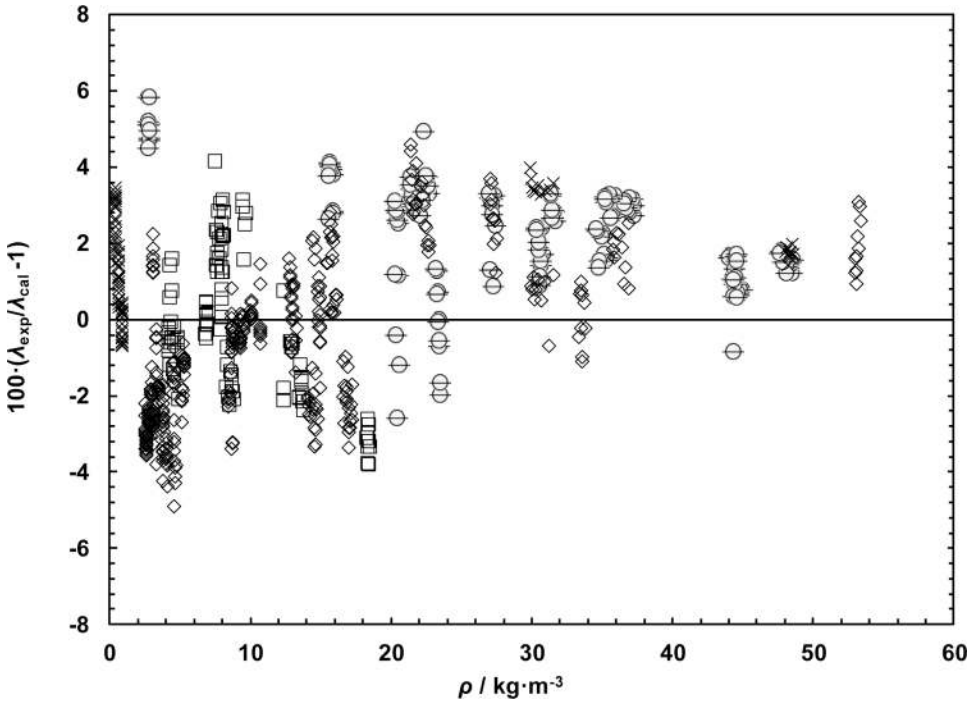

Figure 3.

Relative deviation between the present experimental data (⊖, double-wire transient vapor; ◇, double-wire steady-state vapor; ×, single-wire supercritical;, single-wire transient vapor) and the correlation for the thermal conductivity of Novec 649 as a function of density for the gas phase at pressures up to 1 MPa.

NIST Author Manuscript

NIST Author Manuscript

NIST Author Manuscript

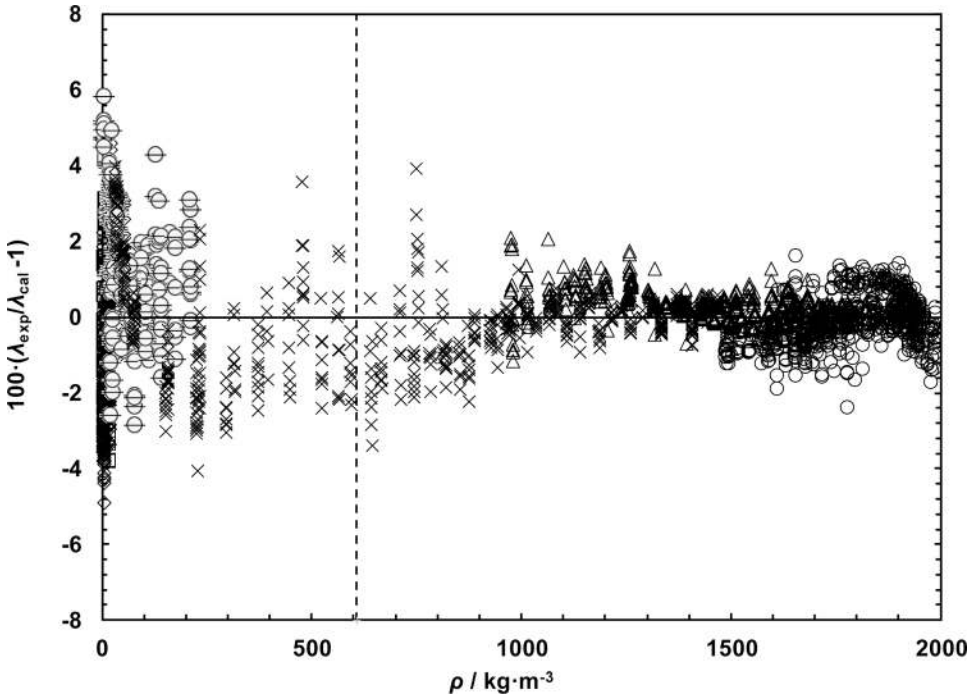

Figure 4.

Relative deviation between the present experimental data and the correlation for the thermal conductivity of Novec 649 as a function of density:, double-wire transient vapor; ◇, double-wire steady-state vapor; O, double-wire transient liquid;×, single-wire supercritical; ⊖, single-wire transient vapor; Δ, single-wire transient liquid. The critical density is designated by the dashed line.

NIST Author Manuscript

NIST Author Manuscript

NIST Author Manuscript

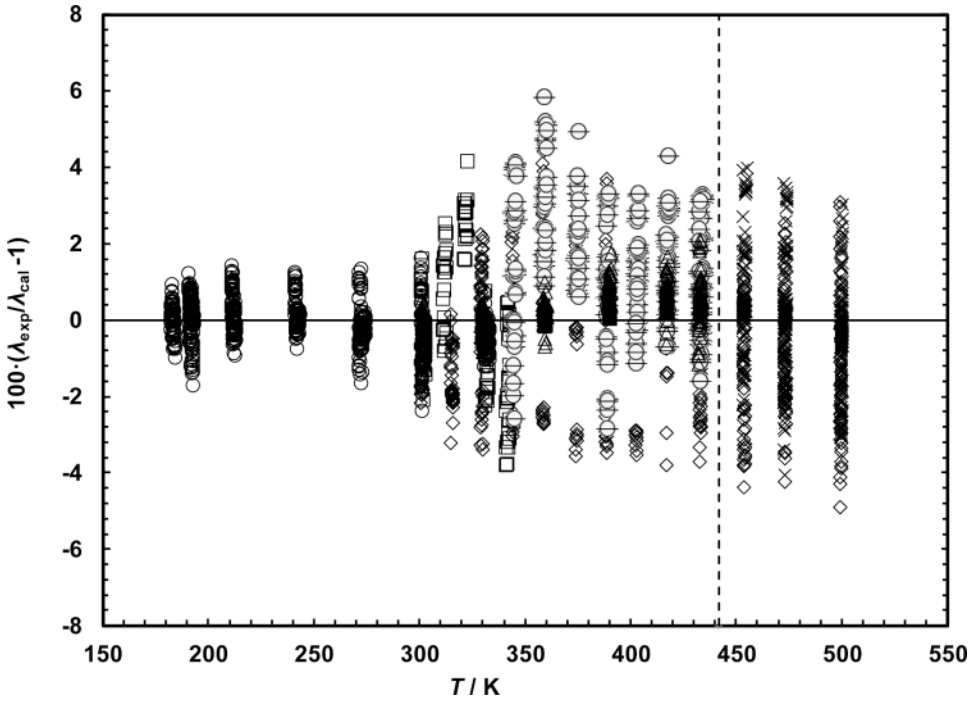

Figure 5.

Relative deviation between the present experimental data and the correlation for the thermal conductivity of Novec 649 as a function of temperature:, double-wire transient vapor; ◇, double-wire steady-state vapor; O, double-wire transient liquid;×, single-wire supercritical; ⊖, single-wire transient vapor; Δ, single-wire transient liquid. The critical temperature is designated by the dashed line.

NIST Author Manuscript

NIST Author Manuscript

NIST Author Manuscript

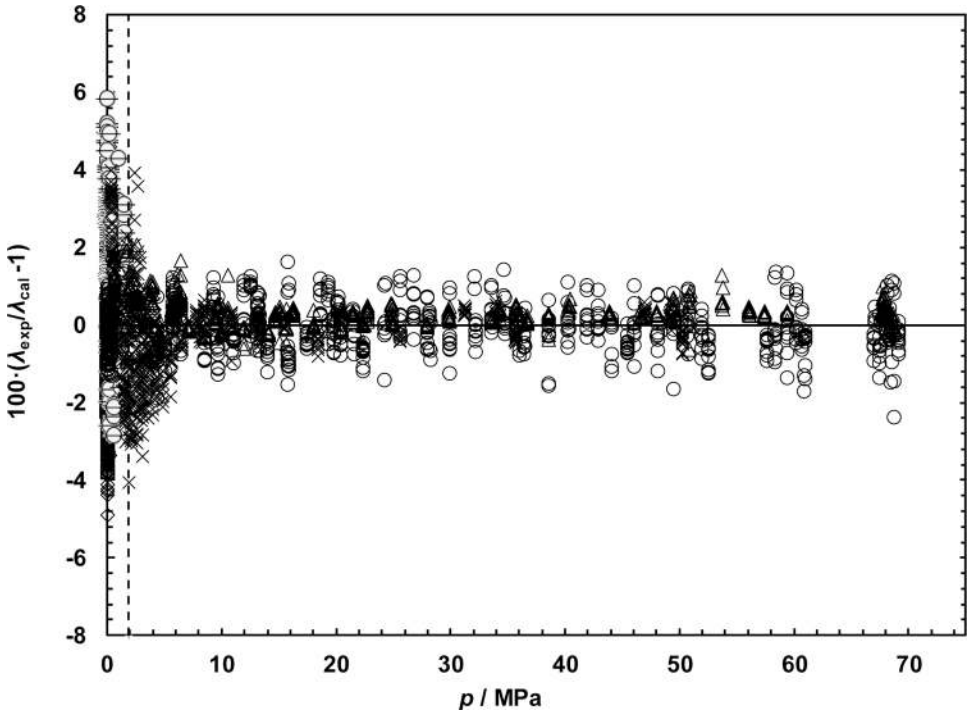

Figure 6.

Relative deviation between the present experimental data and the correlation for the thermal conductivity of Novec 649 as a function of pressure:, double-wire transient vapor; ◇, double-wire steady-state vapor; O, double-wire transient liquid;×, single-wire supercritical;, single-wire transient vapor; Δ, single-wire transient liquid. The critical pressure is designated by the dashed line.

NIST Author Manuscript

NIST Author Manuscript

NIST Author Manuscript

Table 1.

Sample Summary Table.

Chemical Name	Source	Initial Mole Fraction Purity	Purification Method	Final Mole Fraction Purity	Analysis Method
1,1,1,2,2,4,5,5,5-nonafluoro-4-(trifluoromethyl)-3-pentanone[a]	3M	0.9995	Freeze-Thaw Degassing	0.9995[b]	GC-Mass Spectrometry-IR Analysis + Karl Fischer Titration

[a] Also known as FK-5-1-12, Novec 649, Novec 1230 with CAS number 756-13-8.

[b] Impurities of 0.0005 mole fraction 1,1,1,2,3,3,3-heptafluoropropane and less than 25×10^{-6} mole fraction water.

NIST Author Manuscript

NIST Author Manuscript

NIST Author Manuscript

Table 2.

Parameters for the dilute-gas and residual thermal conductivity of Eqs. 4 and 5 for Novec 649.

Dilute-Gas Thermal Conductivity of Eq 4	
k	A_k /(W m^{-1} K^{-1})
0	1.54022×10^{-3}
1	-15.0745×10^{-3}
2	49.0451×10^{-3}
3	-60.7192×10^{-3}
4	46.2647×10^{-3}
5	-3.16935×10^{-3}
j	a_j /(W m^{-1} K^{-1})
0	−0.211741
1	1.16696
2	−1.15574
3	1.0

Residual Thermal Conductivity of Eq 5		
i	j	B_{ij} /(W m^{-1} K^{-1})
1	1	−0.0234542
1	2	0.0158544
2	1	0.0418017
2	2	−0.0334181
3	1	−0.0274745
3	2	0.0282766
4	1	0.00932188
4	2	−0.0103009
5	1	−0.00111766
5	2	0.00147852

NIST Author Manuscript

NIST Author Manuscript

NIST Author Manuscript

Table 3.

Values of thermal conductivity calculated for Novec 649 with the correlation (Eq. 3 to 9) at specified T and ρ, with the coefficients in Table 2. The value of viscosity used for T=445 K and ρ =685.0 kg m^{-3} is 68.836 μPa s, calculated with the correlation of Wen et al.[10]

T / K	ρ/(kg m^{-3})	p/MPa*	λ/(W m^{-1} K^{-1})
300.0	0.00	0.00	0.011876
300.0	5.50	0.04	0.011813
300.0	1673.3	20.02	0.065259
445.0	0.00	0.00	0.022632
445.0	685.0	2.00	0.036508
445.0	685.0	2.00	0.024976**

*Pressures calculated with the equation of state of McLinden et al.[8]

**Calculated with critical enhancement = 0.